CHAPTER

6

EXTERNALLY FINNED TUBES

6.1 INTRODUCTION

Finned-tube heat exchangers have been used for heat exchange between gases and liquids (single or two phase) for many years. Figure 6.1a and b shows two important finned-tube heat exchanger construction types. Figure 6.1a is the plate fin-and-tube geometry, and Figure 6.1b shows individually finned tubes. Although round tubes are shown in Figure 6.1, oval or flat tubes are also used, for example, in automotive radiators. A plain air-side geometry is shown in the Figure 6.1 geometries. Figure 6.1a and b show a staggered tube arrangement, which provides higher performance than an inline tube arrangement. Externally finned tubes are also frequently used for liquids. Figure 6.1c shows an integral-fin tube used for liquids. However, extended surfaces for liquids typically use lower fin height than for gases. Because liquids have higher heat transfer coefficients than gases, fin efficiency considerations require shorter fins with liquids than with gases. When used with liquids, the fin height is typically in the 1.5 to 3 mm range. The dominant amount of material in this chapter is applicable to high fins, which are used for gases.

Because the gas-side heat transfer coefficient is typically much smaller than the tube-side value, it is important to increase the air-side hA-value. A plain surface geometry will increase the air-side hA value by increasing the area (A). Use of enhanced fin surface geometries will provide higher heat transfer coefficients than a plain surface. To maintain reasonable friction power with low-density gases, the gas velocity is usually less than 5 m/s.

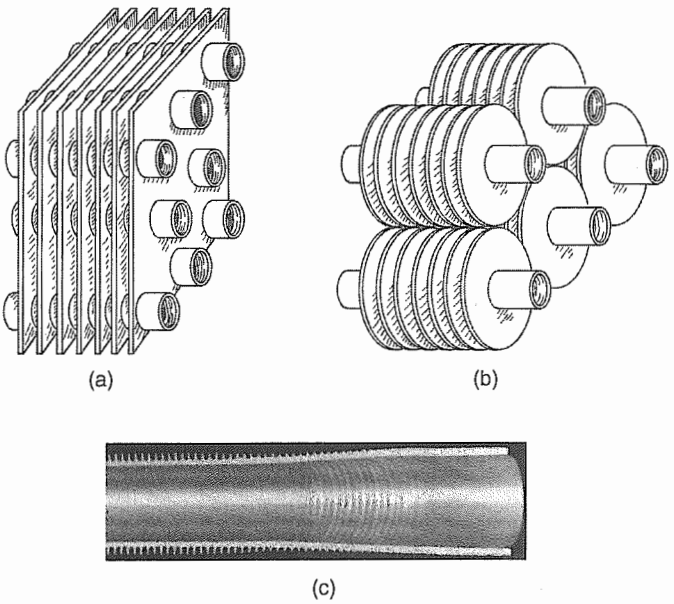

Figure 6.1 Finned tube geometries used with circular tubes: (a) plate fin-and-tube used for gases, (b) individually finned tube having high fins, used for gases. (From Webb [1987]) (c) Low, integral-fin tube.

Important basic enhancement geometries include wavy and interrupted fins. Variants of the interrupted strip fin are also used with finned-tube heat exchangers for heat exchange to a tube-side fluid. Figure 6.2 shows four variants of the interrupted strip fin applied to gas-fluid heat exchangers. Figure 6.2a through d are applied to circular tubes, and Figure 6.2e and f are used with flat, extruded aluminum tubes. These extruded tubes have internal membranes for pressure containment. Figure 6.2a through 6.2d are commonly used in commercial air-conditioning equipment. In Figure 6.2a, the segmented aluminum fin (or "spine fin") is spiral-wound on the tube, and is affixed using an adhesive as described by Abbott et al. [1980] and by Webb [1983a, 1987]. In Figure 6.2b through d, a copper or aluminum tube is mechanically expanded on aluminum plate fins. The Figure 6.2e version is typically made with aluminum fins brazed on flat extruded aluminum tubes. Figure 6.2f shows the "skive fin" design, as described by O'Connor and Pasternak [1976], for which the fins are slit from the thick wall of an aluminum extrusion and bent upward. These constructions are described by Webb [1983a, 1987], and Shah and Webb [1982]. The Figure 6.2e and f geometries on flat aluminum tubes have not found wide commercial acceptance as that of the Figure 6.2a through 6.2d geometries for residential air-conditioning applications. This may be due in part to the cost of brazing or of the extruded tubes. However, the Figure 6.2e and f designs have been recently introduced for use in automotive air-conditioning evaporators and condensers. Recent developments in automotive brazed aluminum manufacturing technology have made the costs of the Figure 6.2e heat exchanger construction more favorable.

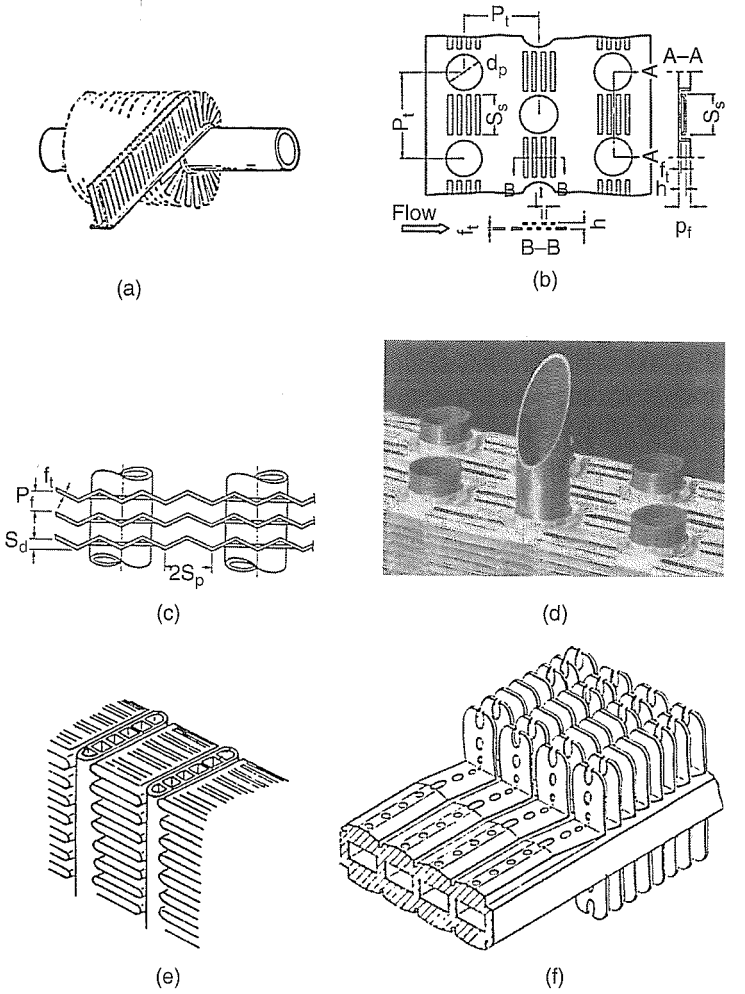

Figure 6.2 Air-side geometries used in finned tube heat exchangers: (a) spine-fin, (b) slit type OSF, (c) wavy fins, (d) convex louver fin, (e) Louver fins brazed to extruded aluminum tube, (f) interrupted skive fin integral to extruded aluminum tube.

Figure 6.14c shows a recent fin design, where winglet-type vortex generators are formed radially (see Section 6.5.7).

Because the gas-side heat transfer coefficient may be 5 to 20% that of the tube-side fluid, the use of closely spaced, high fins is desirable. High fin efficiency can be obtained, if the fin material has high thermal conductivity, e.g., aluminum or copper. If steel fins are required, fin efficiency considerations will dictate shorter or thicker fins. Operational constraints, such as gas-side fouling may limit the fin density. Air-conditioning applications use 500 to 800 fins/m while process air coolers are usually limited to 400 fins/m. Dirty, soot-laden gases may limit the fin

density to 200 fins/m. Different correlations are required for the Figure 6.1a and b geometries.

The fin material used also depends on the operating temperature and the corrosion potential. Listed below are the fin and tube materials used in a variety of applications:

1. Residential air conditioning: Aluminum fins and copper or aluminum tubes
2. Automotive air conditioning: Aluminum fins and aluminum tubes
3. Automotive radiators: Aluminum fins brazed to aluminum tubes, or copper fins soldered to brass tubes
4. Process industry heat exchangers: Air-cooled condensers that may use aluminum fins on copper or steel tubes
5. Boiler economizers and heat-recovery exchangers: Steel fins on steel tubes required by the higher operating temperature

In addition to describing the various fin geometries and their performance characteristics, this chapter compares the performance of alternative heat exchanger and fin configurations. Then heat exchanger and enhanced fin geometries that will yield the highest performance per unit heat exchanger core weight are identified. Finally, possible improvements in the air-side surface geometry are considered.

6.2 THE GEOMETRIC PARAMETERS AND THE REYNOLDS NUMBER

6.2.1 Dimensionless Variables

The flow pattern in finned-tube heat exchangers is very complex, due to its three-dimensional nature and flow separations. The use of enhanced fin geometries introduces further complications. Good progress has been made in attempts to analytically or numerically predict the heat transfer coefficient and friction factor. The numerical achievements on finned tubes are discussed in Section 6.11.

Equations to predict the heat transfer coefficient and friction factor are usually based on power-law correlations using multiple regression techniques. Use of this method requires that one know the geometric and flow variables involved. The geometric and flow variables that affect the heat transfer coefficient and friction factor are the following.

1. Flow variables: Air velocity (u), viscosity (μ), density (ρ), thermal conductivity (k), and specific heat (c_p).
2. Tube bank variables: Tube root diameter (d_o), transverse tube pitch (S_t), row pitch (S_l), tube layout (staggered or inline), and the number of rows (N).
3. Fin geometry variables: For a plain fin, these are the fin pitch (p_f), fin height (e), fin thickness (t). If, for example, an enhanced wavy fin geometry is used the added variables are the wave height (e_w), the wave pitch (p_w), and the wave shape.

Thus, there are seven geometry variables for a plain fin (excluding the tube layout) and five flow variables. Two additional variables are introduced to account for the wavy fin geometry. Dimensional analysis specifies that the number of possibly important dimensionless groups is the number of variables minus the number of dimensions. Because four dimensions are involved for heat transfer (mass, length, time, and heat transfer), there are eight dimensionless variables for the plain fin and ten dimensionless variables for the wavy fin. The dimensionless flow variables typically used in correlations are the Reynolds number and the Prandtl number. For heat transfer, one has the Nusselt number or the Stanton number. For pressure drop, one uses the friction factor.

There are no "rules" for selecting the appropriate dimensionless geometric variables. This is simply "cut-and-try" to select the ones that give the best correlation of the data set. Further, power-law correlations have no rational basis and provide only an empirical correlation of the data set. It is dangerous to extrapolate such correlations beyond the range of the variables used to develop the correlation.

6.2.2 Definition of Reynolds Number

The basic definition of the Reynolds number is $L_c G/\mu$, where L_c is a characteristic dimension and G is usually defined as the mass velocity in the minimum flow area. For fully developed flow inside a plain tube, there is only one possible characteristic dimension — the tube diameter. As previously stated, there are seven dimensions associated with a plain fin geometry, and nine for the wavy fin geometry. Hence, there is no unique characteristic dimension. Hence, there are eight possible values of L_c for definition of the Reynolds number of the plain fin geometry. One approach to defining Reynolds number is to identify a characteristic dimension that appears to dominate over the other possible choices. For a bare tube bank, the possible choices are S_t, S_l, and d_o. However, there is no uniform agreement on the characteristic dimension used to define the Reynolds number. Two different characteristic dimensions have been used to define L_c in the Reynolds number. They are the tube diameter (d_o) or the hydraulic diameter (D_h). Kays and London [1984] choose to use the hydraulic diameter for the characteristic dimension for all situations, including bare and finned-tube banks. There is no evidence to suggest that hydraulic diameter is a better choice. In fact, there is evidence that the tube diameter may be a better choice for finned-tube banks. This is shown later. The conclusion is that the choice of characteristic dimension is arbitrary.

For fully developed flow in tubes, one defines laminar and turbulent regimes. Do such regimes also exist for finned-tube banks? To evaluate this, consider the case of the Figure 6.1a geometry. Assume that the geometry uses d_o = 19 mm with an equilateral triangular pitch of S_t = 44.45 mm, and 472 fins/m with 0.2 mm thickness. Assume air enters the exchanger at 3 m/s and 20°C. The mass velocity in the minimum flow area (G) is 7.34 kg/m^{2}s and the hydraulic diameter is 3.68 mm. The Reynolds numbers based on d_o and D_h are 8710 and 1640, respectively. Is the flow laminar or turbulent? Based on $\mathrm{Re}_{\mathrm{Dh}}$, one would say it is laminar. But, based on tube diameter (Re_d), one would say it is turbulent. In reality, it exhibits some of both characteristics.

If the tubes were not present, the flow geometry would be a parallel plate channel, for which D_h = 3.82 mm. The Reynolds number is 1588, which is clearly laminar. However, the tubes shed eddies, which wash over the fin surface and provide mixing of the flow.

If the Reynolds number based on hydraulic diameter were dominant over the Reynolds number based on tube diameter, one would expect that the Nu and f data for different fin pitches would tend to fall on one line. It is shown below that this is not the case.

6.2.3 Definition of the Friction Factor

This book strives to use only the Fanning friction factor (f), defined in the Nomenclature at the end of the chapter. However, other friction factor definitions are frequently used for tube banks (bare and finned). A common definition for tube banks is given the symbol f_{tb}. It is related to the Fanning friction factor by the equation

$$f_{tb}N = \frac{fL}{D_h} \tag{6.1}$$

where N is the number of tube rows in the flow direction and L is the flow depth. For bare or finned tubes, $L = S_l\,(N - 1) + d_e$, where d_e is diameter over the fins. For a bare tube bank, $d_e = d_o$.

6.2.4 Sources of Data

Much of the data on finned tube heat exchangers were developed by industrial organizations, and is thus proprietary. However, some have been published in the open literature. There are two sources for compilations of published data. One is the book by Kays and London [1984] and a report by Rozenman [1976a]. Both are relatively old, and do not contain state-of-the-art data on enhanced surfaces. Kays and London present data for 22 geometries and Rozenman provides data for 161 geometries. The data of both authors are presented in the format of j and f vs. Re_{Dh}, and complete geometry details are provided. Rozenman [1976b] provides empirical correlations for j and f vs. Re_{Dh}. Since publication of these two references, various journal and conference publications have provided additional data on numerous geometries, including enhanced fin designs. These data are discussed in the following sections.

6.3 PLAIN PLATE-FINS ON ROUND TUBES

Figure 6.1a shows the finned-tube geometry with continuous, plain plate fins in a staggered tube layout. An inline tube geometry is seldom used because it provides substantially lower performance than the staggered tube geometry. The performance difference between inline and staggered tube layouts is discussed in Section 6.8.

6.3.1 Effect of Fin Spacing

Rich [1973] measured heat transfer and friction data for the Figure 6.1a geometry having plain fins, four rows deep, on 12.7-mm-diameter tubes equilaterally spaced on 32-mm centers. The tubes and fins were made of copper, and the fins were solder-bonded to minimize contact resistance. The geometry of all heat exchangers was identical, except the fin density ($1/p_f$), which was varied from 114 to 811 fins/m. All fins were 0.25 mm thick.

Figure 6.3 shows the friction factor and the Colburn j factor ($StPr^{2/3}$) data (smoothed curve fit) as a function of Reynolds number (based on D_h) for the eight fin spacings tested. Entrance and exit losses were subtracted from the pressure drop, and are not included in the friction factor. Figure 6.3 clearly shows that the hydraulic diameter based Re (Re_{Dh}) does not correlate either the j or f data.

Rich proposed that the friction drag force is the sum of the drag force on a bare tube bank (Δp_t) and the drag caused by the fins (Δp_f). The difference between the total drag force and the drag force associated with the corresponding bare tube bank is the drag force on the fins. Thus, the friction component resulting from the fins is given by

$$f_f = (\Delta p - \Delta p_t)\,\frac{2A_c\rho}{G^2A_f} \tag{6.2}$$

The term Δp_t is that measured for a bare tube bank of the same geometry, without fins. Both Δp drop contributions are evaluated at the same minimum area mass

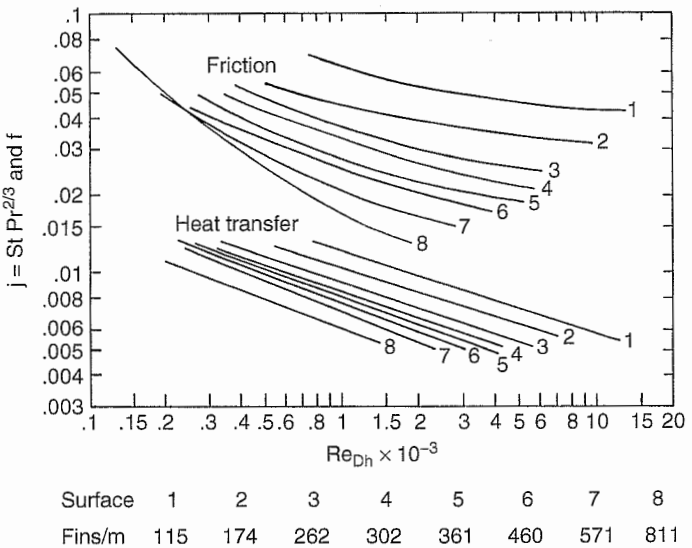

Figure 6.3 Heat transfer and friction characteristics of a four-row plain plate fin heat exchanger for different fin spacings.

velocity. Figure 6.4 shows the same j factor data and the fin friction factor calculated by Equation 6.2 plotted vs. the Reynolds number based on the longitudinal row pitch (S_l). The row pitch (S_l) is constant for all of the test geometries. Figure 6.4 shows that the j factor is a function of velocity in the minimum flow area (G_c), and is essentially independent of fin spacing. At the same mass velocity (G_c), the bare tube bank heat transfer coefficient is 40% larger than that of the finned-tube bank. Figure 6.4 shows that the resulting friction correlation is reasonably good, except for the closest fin spacings. The friction factor data of surfaces 7 and 8 may be questionable, since these surfaces show smaller j/f values than for the other fin spacings. This behavior is unexpected. Normally, the j/f ratio will increase as the fin spacing is reduced, because the fractional parasitic drag associated with the tube is reduced. Use of the Reynolds number based on S_l has no real significance, as all geometries tested had the same S_l. The same degree of correlation would result from use of a Reynolds number based on the tube diameter (d_o), which was also constant. Figure 6.4 may be regarded as evidence that the Reynolds number based on hydraulic diameter will not correlate the effect of fin pitch.

In a later study, Rich [1975] used the same heat exchanger geometry with 551 fins/m to determine the effect of the number of tube rows on the j factor. Figure 6.5 shows the average j factor (smoothed data fit) for each exchanger as a function of Re_{Sl}. The numbers on the figure indicate the number of rows in each coil. The row effect is greatest at low Reynolds numbers and becomes negligible at $Re_{Sl} > 15{,}000$.

Following Rich [1973, 1975], a number of studies have been performed on plain finned-tube heat exchangers (McQuiston [1978], Seshimo and Fujii [1991], Kayansayan [1993], Wang et al. [1996b], Abu Madi et al. [1998], Yan and Sheen [2000],

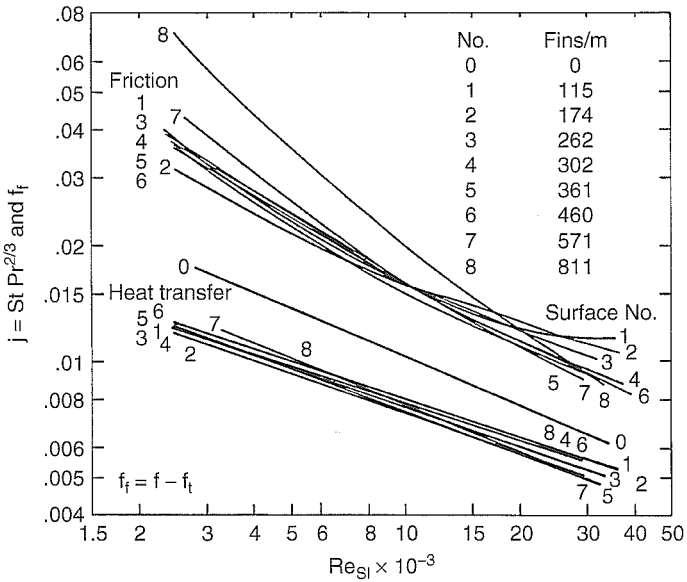

Figure 6.4 Plot of the j factor and the fin friction vs. Re_{Sl}.

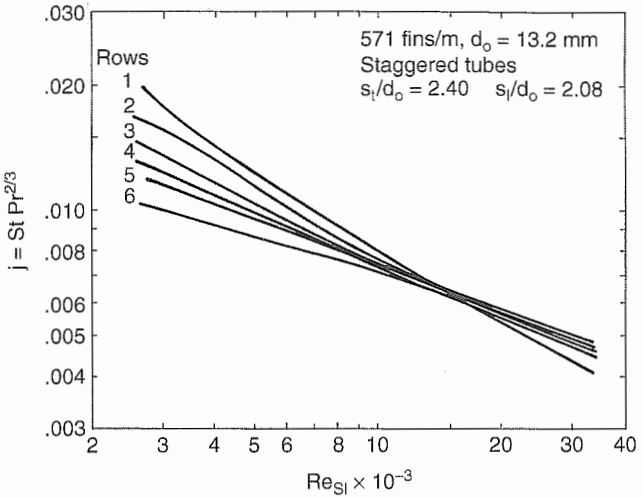

Figure 6.5 Average heat transfer coefficients for plain plate-finned tubes (571 fins/m) having one to six rows. Same geometry dimensions as Figure 6.4.

Wang and Chi [2000]). These studies generally confirmed Rich's observation that the j factor shows negligible effect of fin pitch, but does show significant row effect at low Reynolds numbers. Wang et al. [1996b] and Wang and Chi [2000] reported that the friction factor is independent of the number of tube rows.

6.3.2 Correlations for Staggered Tube Geometries

Correlations to predict the j and f factors vs. Reynolds number for plain fins on staggered tube arrangements were developed by McQuiston [1978], Gray and Webb [1986], Kim et al. [1999], and Wang et al. [2000a]. The McQuiston correlation is based on the data of Rich [1973, 1975] shown on Figure 6.3 and Figure 6.5, and three other investigators. Gray and Webb used the same data set as McQuiston, plus that of two additional investigators. The McQuiston and the Gray and Webb heat transfer correlations are comparable in accuracy. However, the Gray and Webb friction factor correlation is much more accurate than that of McQuiston.

The Gray and Webb [1986] heat transfer correlation (for four or more tube rows of a staggered tube geometry) is

$$j_4 = 0.14\,\mathrm{Re}_d^{-0.328}\left(\frac{S_t}{S_l}\right)^{-0.502}\left(\frac{s}{d_o}\right)^{0.031} \tag{6.3}$$

Equation 6.3 assumes that the heat transfer coefficient is stabilized by the fourth tube row, hence the j factor for more than four tube rows is the same as that for a four-row exchanger. The correction for rows less than four is based on correlation of the Figure 6.5 data, and is given by

$$\frac{j_N}{j_4} = 0.991\left[2.24\,\mathrm{Re}_d^{-0.092}\left(\frac{N}{4}\right)^{-0.031}\right]^{0.607(4-N)} \tag{6.4}$$

Equations 6.3 and 6.4 correlated 89% of the data for 16 heat exchangers within ±10%. The McQuiston [1978] correlation gives comparable results.

The Gray and Webb [1986] friction correlation assumes that the pressure drop is composed of two terms. The first term accounts for the drag force on the fins, and the second term accounts for the drag force on the tubes. The validity of this model was previously established in the discussion of Figure 6.4. The friction factor of the heat exchanger is given by

$$f = f_f\frac{A_f}{A} + f_t\left(1-\frac{A_f}{A}\right)\left(1-\frac{t}{p_f}\right) \tag{6.5}$$

The friction factor associated with the fins (f_f) is given by Equation 6.6:

$$f_f = 0.508\ \mathrm{Re}_d^{-0.521}\left(\frac{S_t}{d_o}\right)^{1.318} \tag{6.6}$$

The friction factor associated with the tubes (f_t) is obtained from a correlation for flow normal to a staggered bank of plain tubes. Gray and Webb used the Zukauskas [1972] tube bank correlation, also given in Incropera and DeWitt [2001], to calculate the tube bank contribution, Δp_t. The f_t is calculated at the same mass velocity (G) that exists in the finned-tube exchanger. Equation 6.5 correlated 95% of the data for 19 heat exchangers within ±13%. The equation is valid for any number of tube rows. McQuiston [1978] also developed a friction correlation using the same data set; however, his friction correlation has quite high error limits, +167/–21% for the same data.

The range of dimensionless variables used in the development of the Gray and Webb correlations are $500 \le \mathrm{Re}_d \le 24{,}700$, $1.97 \le S_t/d_o \le 2.55$, $1.7 \le S_l/d_o \le 2.58$ and $0.08 \le s/d_o \le 0.64$.

Recent work by Seshimo and Fujii [1991] provides more generalized correlations for staggered banks of plain fins having one to five tube rows. They tested 35 heat exchangers, having systematically changed geometric parameters. They used three tube diameters (6.35, 7.94, and 9.52 mm) with the multirow designs using an equilateral triangular pitch. Data were obtained for four fin densities, from 454 to 1000 fins/m. They tested one-row designs with different transverse tube pitch and fin depth and show that the one- and two-row data may be separately correlated using an entrance length parameter. Their data were correlated using a Reynolds number (Re_{Dv}) defined in terms of the volumetric hydraulic diameter (D_v). The D_v is given by

$$D_v = \frac{4A_mL}{A} \tag{6.7}$$

where $A_m L$ is defined as the total volume of the exchanger, less the volume of the tube bank. The one- and two-row data were correlated in terms of the entrance length parameter, $X_{Dv}^{+} \equiv \mathrm{Re}_{Dv}\mathrm{Pr}D_v/L$. The correlations are

$$\mathrm{Nu} = 2.1(X_{Dv}^{+})^{n} \tag{6.8}$$

$$fLD_v = c_1 + c_2(X_{Dv}^{+})^{-m} \tag{6.9}$$

where the constants and exponents differ for one- or two-row exchangers:

1. One-Row: $n = 0.38$, $m = 1.07$, $c_1 = 0.43$, and $c_2 = 35.1$.
2. Two-Row: $n = 0.47$, $m = 0.89$, $c_1 = 0.83$, and $c_2 = 24.7$.

For three or more rows, these entrance length-based correlations did not work very well over the entire Reynolds number range ($200 < \mathrm{Re}_{Dh} < 800$), because vortex shedding from the tubes seems to be an important factor. For $\mathrm{Re}_{Dh} > 400$, the data were correlated using conventional Nusselt number and Reynolds number (Re_{Dh}) and flow based on the minimum flow area. For $\mathrm{Re}_{Dh} < 400$, the one-row variant of Equations 6.8 and 6.9 correlated the data for one to five rows.

Historically, one finds that the tube diameter used in finned-tube heat exchangers is decreasing. Some window air conditioners use tube diameters as small as 5.0 mm. Kim et al. [1999] improved the Gray and Webb [1986] correlation by including the data of Wang and Chi [2000] and Youn [1997] for heat exchangers having 7-mm-diameter tubes. The Kim et al. correlation predicted the data for tube diameters larger than 7 mm with approximately the same accuracy as Gray and Webb [1986]. However, the improvement was significant for the 7-mm tube data. Another general correlation has been developed by Wang et al. [2000a], which includes tube diameters as small as 6.7 mm. The Kim et al. and Wang et al. correlations were compared at $\mathrm{Re}_d = 2500$ for $1 \le N \le 3$, $1.3 \le p_f \le 3.0$ mm. For heat exchangers having 9.5-mm-OD tubes, the predicted j factors by Kim et al. correlation agree with those by Wang et al. correlation within 10%. For the 7.0-mm tube configuration, the two correlations yielded approximately the same j factors for $N = 3$. However, the difference increased as the row number decreased. Kim et al. correlation generally predicts larger friction factors than Wang et al. correlation. The Kim et al. [1999] correlation (for three or more tube rows) is

$$j_3 = 0.163\,\mathrm{Re}_d^{-0.369}\left(\frac{S_t}{S_l}\right)^{0.106}\left(\frac{s}{d_o}\right)^{0.0138}\left(\frac{S_t}{d_o}\right)^{0.13} \qquad (N \ge 3) \tag{6.10}$$

$$\frac{j_N}{j_3} = 1.043\left[\mathrm{Re}_d^{-0.14}\left(\frac{S_t}{S_l}\right)^{-0.564}\left(\frac{s}{d_o}\right)^{-0.123}\left(\frac{S_t}{d_o}\right)^{1.17}\right]^{(3-N)} \qquad (N = 1,2) \tag{6.11}$$

$$f_f = 1.455 \mathrm{Re}_d^{-0.656} \left(\frac{S_t}{S_l}\right)^{-0.347} \left(\frac{s}{d_o}\right)^{-0.134} \left(\frac{S_t}{d_o}\right)^{1.23} \tag{6.12}$$

Kim et al. used the Jakob [1938] correlation for the friction factor due to tubes (f_t), which is

$$f_t = \frac{\pi}{4}\left(0.25 + \frac{0.118}{[S_t / d_o - 1]^{1.08}} \mathrm{Re}_d^{-0.16}\right)\left[\left(\frac{S_t}{d_o}\right) - 1\right] \tag{6.13}$$

Equation 6.5 is used to calculate the friction factor of the heat exchanger.

6.3.3 Correlations for Inline Tube Geometries

Schmidt [1963] reports data and a correlation for the inline geometry. However, little use exists for an inline tube arrangement. This is because tube bypass effects substantially degrade the performance of an inline tube arrangement. The degree of performance degradation for inline circular fins is discussed in Section 6.4.1.

6.4 PLAIN INDIVIDUALLY FINNED TUBES

6.4.1 Circular Fins with Staggered Tubes

Extruded fins or helically wrapped fins on circular tubes, as shown by Figure 6.1b, are frequently used in the process industries and in combustion heat-recovery equipment. Both plain and enhanced fin geometries are used. A staggered tube layout is used, especially for high fins ($e/d_o > 0.2$). A substantial amount of performance data has been published, and several heat transfer and pressure drop correlations have been proposed. The dominant amount of data was taken with a staggered tube arrangement, six or more tube rows deep. The correlations must account for the three tube bank variables (d_o, S_t, and S_l), the fin geometry variable (t, e, and s), and the number of tube rows. Webb [1987] provides a survey of the published data and correlations.

The recommended correlations for a staggered tube layout are made by Briggs and Young [1963] for heat transfer and Robinson and Briggs [1966] for pressure drop. Both correlations are empirically based and are valid for four or more tube rows. The heat transfer correlation is

$$j = 0.134\ \mathrm{Re}_d^{-0.319} \left(\frac{s}{e}\right)^{0.2} \left(\frac{s}{t}\right)^{0.11} \tag{6.14}$$

Equation 6.10 is based on airflow over 14 equilateral triangular tube banks and covers the following ranges: $1100 \le \mathrm{Re}_d \le 18{,}000$, $0.13 \le s/e \le 0.63$, $1.0 \le s/t \le 6.6$, $0.09 \le e/d_o \le 0.69$, $0.01 \le t/d_o \le 0.15$, $1.5 \le S_l/d_o \le 8.2$. The standard deviation was 5.1%.

The isothermal friction correlation of Robinson and Briggs [1966], which we have rewritten in terms of the tube bank friction factor, is

$$f_{tb} = 9.47\,\mathrm{Re}_d^{-0.316}\left(\frac{S_t}{d_o}\right)^{-0.927}\left(\frac{S_t}{S_d}\right)^{0.515} \tag{6.15}$$

Equation 6.15 is based on isothermal airflow data over 17 triangular pitch tube banks (15 equilateral and 2 isosceles). The data span the ranges $2000 \le \mathrm{Re}_d \le 50{,}000$, $0.15 \le s/e \le 0.19$, $3.8 \le s/t \le 6.0$, $0.35 \le e/d_o \le 0.56$, $0.01 \le t/d_o \le 0.03$, $1.9 \le S_t/d_o \le 4.6$. The standard deviation of the correlated data was 7.8%. Equation 6.11 is recommended with strong reservations, because it does not contain any of the fin geometry variables (e, s, or t). Because only a small range of s/e was covered in the tests, it is probable that the correlation will fail outside the s/e range used for developing the correlation. Gianolio and Cuti [1981] compared their data for 17 tube bank geometries containing 1 to 6 rows with the Briggs and Young [1963] and the Robinson and Briggs [1966] correlations. For induced draft, their six-row data are 0 to 10% above that of Briggs and Young. Their data for $N < 6$ were increasingly underpredicted as the number of rows decreases. For $N < 6$, they recommended that the Briggs and Young value be multiplied by the factor $(1 + G/\rho N^2)^{-0.14}$, where G is in kg/m^{2}s units. Gianolio and Cuti [1981] also state that their induced draft h values are 10 to 40% higher than those for forced draft. No explanation is provided for this unexpected result. The Robinson and Briggs [1966] correlation did not predict their data very well.

Although the data on which Equation 6.14 is based included low fin data, e.g., $e/d_o < 0.1$, Rabas et al. [1981] developed more accurate j and f correlations for low fin heights and small fin spacings. The correlations are given below with the exponents rounded off to two significant digits.

$$j = 0.292\left(\frac{d_o G_c}{\mu}\right)^n\left(\frac{s}{d_o}\right)^{1.12}\left(\frac{s}{e}\right)^{0.26}\left(\frac{t}{s}\right)^{0.67}\left(\frac{d_e}{d_o}\right)^{0.47}\left(\frac{d_e}{t}\right)^{0.77} \tag{6.16}$$

where $n = -0.415 + 0.0346(d_e/s)$. The friction correlation is

$$f = 3.805\left(\frac{d_o G_c}{\mu}\right)^{-0.234}\left(\frac{s}{d_e}\right)^{0.25}\left(\frac{e}{s}\right)^{0.76}\left(\frac{d_o}{d_e}\right)^{0.73}\left(\frac{d_o}{S_t}\right)^{0.71}\left(\frac{S_t}{S_l}\right)^{0.38} \tag{6.17}$$

The equations are valid for staggered tubes with $N \ge 6$, $5000 \le \mathrm{Re}_d \le 25{,}000$, $1.3 \le s/e \le 1.5$, $0.01 \le s/t \le 0.06$, $e/d_o \le 0.10$, $0.01 \le t/d_o \le 0.02$, and $1.3 \le S_t/d_o \le 1.5$. The equations predicted 94% of the j data and 90% of the f data within ±15%. Rabas and Taborek [1987] present a survey of correlations, row correction factors, and other issues concerning low, integral-fin tube banks. They compare the ability of Equations 6.11 and 6.17 to predict other data sets, e.g., Groehn [1977]. Other correlations have been developed by Groehn [1977] and ESDU [1985], which were tested to higher Re_d. Apparently, no correlations exist for $\mathrm{Re}_d \le 1000$.

A staggered tube layout gives higher values for j at the same Re_d, especially for high fins ($e/d_o > 0.3$). Hence, the inline tube layout is not recommended for $e/d_o > 0.3$. Rabas and Huber [1989] discuss the reduction of the j factor with increased number of tube rows. Designers interested in inline finned-tube banks should refer to Schmidt [1963], who developed a heat transfer correlation based on data from 11 sources.

6.4.2 Low Integral-Fin Tubes

The Rabas et al. [1981] correlation given by Equations 6.16 and 6.17 is recommended for a staggered layout of low integral fins. Corresponding equations have not been developed for inline tube layouts. However, Brauer's j data [1964] for the $e/d_o = 0.07$ inline tube bank shown in Figure 6.28 is within 20% of that of a staggered bank having the same e/d_o, S_t/d_o, and S_l/d_o. The inline friction factor was approximately 35% smaller than that of the staggered bank. It appears that the performance decrement of inline banks having low fins, e.g., $e/d_o = 0.1$, is not nearly as severe as for high fins, e.g., $e/d_o = 0.4$.

6.5 ENHANCED PLATE FIN GEOMETRIES WITH ROUND TUBES

The wavy (or herringbone) fin and the offset strip fin (also referred to as parallel louver) geometries are the major enhanced surface geometries used on circular tubes. Figure 6.2c shows the wavy fin geometry applied to circular tubes. This figure shows the geometrical dimensions that influence the heat transfer and friction characteristics. The combination of tubes plus a special surface geometry establishes a very complex flow geometry. The heat transfer coefficient of the wavy fin is typically 50 to 70% greater than that of a plain (flat) fin.

6.5.1 Wavy Fin

There are two basic variants of the wavy fin geometry as illustrated in Figure 6.6. They are the smooth wave and the herringbone configurations. Much work has been done on the herringbone wave geometry. However, very limited work has been done on the smooth wave geometry. Goldstein and Sparrow [1977] used a mass transfer technique to measure local and average mass transfer coefficients on a model having herringbone configuration. At Re = 1000 (based on fin spacing), the wave configuration yielded a 45% higher mass transfer coefficient compared with the plain fin counterpart. They proposed that the enhancement results from Goetler vortices that form on concave wave surfaces.

Beecher and Fagan [1987] published heat transfer data for 20, 3-row plate fin-and-tube geometries having the Figure 6.6a wavy fin geometry. Figure 6.6a defines the geometric parameters of the wavy fin. All cores had staggered tubes with three rows with $S_t/S_l = 1.15$. Two tube diameters were tested, $d_o = 9.53$ and 12.7 mm. The fin pitch was varied from 244 fins/m (6.2 fins/in.) to 510 fins/m (13 fins/in.) with

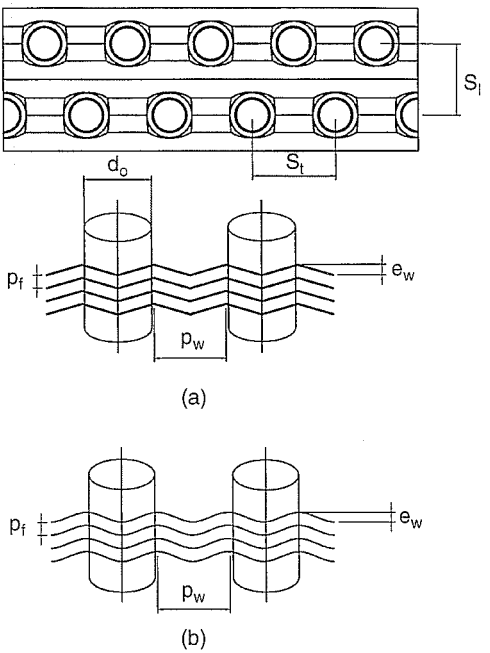

Figure 6.6 Two basic geometries of the wavy fin; (a) herringbone wave, (b) smooth wave.

dimensionless wave heights of $0.076 \le e_w/d_o \le 0.25$ and wave pitches of $0.058 \le e_w/p_w \le 0.346$. The wavy fins have a 3.18-mm-wide (0.125 in.) flat region around the fin collar. The Nusselt number data were presented as Nu_a (= $h_a D_h/k$) vs. the Graetz number, $\mathrm{Gz} = \mathrm{Re}_{\mathrm{Dh}}\mathrm{Pr}D_h/\mathrm{L}$. The Nu_a is based on the arithmetic mean temperature difference (AMTD), rather than the LMTD.

Webb [1990] developed a multiple regression correlation of the Beecher and Fagan [1987] wavy fin data. Because the curve of Nu_a vs. Gz was not a straight line on log-log coordinates, a two-region correlation was used. The correlations are

$$\mathrm{Nu}_a = 0.5\mathrm{Gz}^{0.86}\left(\frac{S_t}{d_o}\right)^{0.11}\left(\frac{s}{d_o}\right)^{-0.09}\left(\frac{e_w}{S_l}\right)^{0.12}\left(\frac{p_w}{S_l}\right)^{-0.34} \qquad \mathrm{Gz} \le 25 \qquad (6.18)$$

$$\mathrm{Nu}_a = 0.83\mathrm{Gz}^{0.76}\left(\frac{S_t}{d_o}\right)^{0.13}\left(\frac{s}{d_o}\right)^{-0.16}\left(\frac{e_w}{S_l}\right)^{0.25}\left(\frac{p_w}{S_l}\right)^{-0.43} \qquad \mathrm{Gz} > 25 \qquad (6.19)$$

For $5 \le \mathrm{Gz} \le 180$, 96% of the data were correlated within ±10%. The Nusselt number is traditionally based on the LMTD rather than the AMTD; however, Beecher and Fagan discovered that, at low air velocities, small errors in air temperature measurement led to large errors in calculation of the LMTD and they chose to base the Nusselt number on the AMTD. The Nu based on the AMTD may be converted to the LMTD-based Nusselt number (Nu_l), by the following equation:

$$\mathrm{Nu}_l = \frac{\mathrm{Gz}}{4} \ln\left(\frac{1+2\mathrm{Nu}_a/\mathrm{Gz}}{1-2\mathrm{Nu}_a/\mathrm{Gz}}\right) \tag{6.20}$$

Much data on the herringbone wave fin geometry were published by Wang and co-workers (Wang et al. [1997b, 1998a, 1999a, 1999d], Abu Madi et al. [1998]), mostly on staggered layout. The effect of fin pitch and the effect of tube rows were generally similar to those of the plain finned tubes. The j factors were approximately independent of the fin pitch. The effect of tube rows, however, was not as pronounced as that of the plain finned tubes. The reason was attributed to the turbulence generated by the wave configuration. The effect of corrugation depth was investigated by Wang et al. [1999d]. The j and f factors increased as the corrugation depth increased. Wang et al. [1997b] provide j and f data on 6 inline geometries with row numbers varying from 2 to 4.

General j and f correlations for the herringbone wave configuration were developed by Kim et al. [1997]. The database included Beecher and Fagan [1987] and Wang et al. [1997b]. A procedure similar to that used by Gray and Webb [1986] was taken for the development of the correlation. Correlations include staggered, as well as inline geometries. For the staggered layout, 92% of the heat transfer data were correlated within ±10%, and 91% of the friction data were correlated within ±15%. Wang et al. [1999c] also provide j and f correlations for the herringbone wave geometry. The correlation has been developed based on their own data. Listed below are the Kim et al. [1997] correlations.

$$j_3 = 0.394\,\mathrm{Re}_d^{-0.357}\left(\frac{S_t}{S_l}\right)^{-0.272}\left(\frac{s}{d_o}\right)^{-0.205}\left(\frac{p_w}{2e_w}\right)^{-0.558}\left(\frac{e_w}{s}\right)^{-0.133} \tag{6.21}$$

$$\frac{j_N}{j_3} = 0.978 - 0.01N \quad \mathrm{Re}_d > 1000 \tag{6.22}$$

$$\frac{j_N}{j_3} = 1.35 - 0.162N \quad \mathrm{Re}_d < 1000 \tag{6.23}$$

$$f_f = 4.467\,\mathrm{Re}_d^{-0.423}\left(\frac{S_t}{S_l}\right)^{-1.08}\left(\frac{s}{d_o}\right)^{-0.034}\left(\frac{p_w}{2e_w}\right)^{-0.672} \tag{6.24}$$

Kim et al. used the Zukauskas [1972] correlation for the friction factor due to tubes (f_f). Equation 6.5 is used to calculate the friction factor of the heat exchanger.

Limited data on the smooth wave configuration are provided Mirth and Ramadhyani [1994] for the staggered tube layout. They tested five heat exchangers with two different wave fin patterns. Three samples had smooth continuous wave fins, while the other two had a relatively flat area between each pair of waves. The samples had four and eight rows. A correlation was developed based on their own data. Youn et al. [1998] provided additional data on two-row heat exchangers.

Kang and Webb [1998] compared j and f factors of the herringbone and the smooth wave geometries. The two configurations had the same wave depth and wave pitch. Data were taken from scaled-up (1.37 times) models. The smooth wave geometry yielded 4% higher j factors and 10% higher f factors. The smooth wavy geometry had an approximate sinusoidal fin pattern.

6.5.2 Offset Strip Fins

The Figure 6.2b OSF concept (also known as "slit fins") has been applied to finned-tube heat exchangers with plain fins for dry cooling towers and for refrigerant condensers. Figure 6.2b shows one such geometry, which was studied by Nakayama and Xu [1983]. Figure 6.7 shows the heat transfer coefficients of the OSF and a plain fin used in a two-row staggered tube heat exchanger having 525 fins/m on 10-mm-diameter tubes. At 3 m/s air velocity, the OSF provides a 78% higher heat transfer coefficient than the plain fin. For the same louver geometry, the OSF will provide a higher heat transfer coefficient, when used in the plate-and-fin-type heat exchanger. The OSF shown in Figure 5.4 provides 150% higher heat transfer coefficient than the plain fin at the same velocity. Comparison of plain fin geometries in Figures 5.4 and 6.7 shows that the heat transfer coefficient of the Figure 6.7 plain fin is 90% greater than that of the Figure 5.4 plain fin geometry. Thus, the flow acceleration and fluid mixing in the wake of the tube provide a substantial enhancement for plain fins on tubes.

Generalized empirical correlations for j and f vs. Re have not been developed for OSF geometry on round tubes. However, Nakayama and Xu [1983] propose an

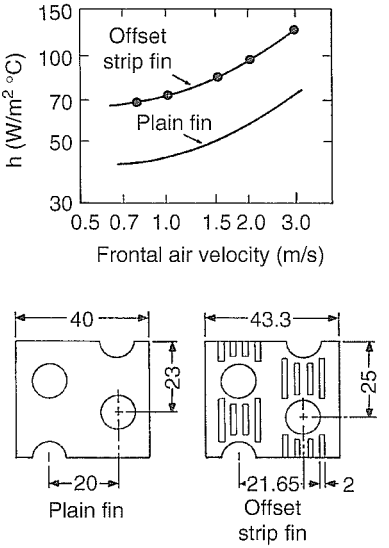

Figure 6.7 Comparison of the heat transfer coefficient for the OSF and plain fin geometries for 9.5-mm-diameter tubes, 525 fins/m, and 0.2-mm fin thickness as reported by Nakayama and Xu [1983].

empirical correlation to define the enhancement level (h/h_p) of an OSF geometry having 2.0-mm strip width (in the flow direction) and 0.2-mm fin thickness.

Recent data on OSF geometry have been provided by Wang and Chang [1998], Wang et al. [1999b], Kang and Webb [1998], Yun and Lee [2000], and Du and Wang [2000]. One important issue of the strip design is the direction of the strip, relative to the airflow direction. Radial strips will provide better heat conduction path compared with the normal strips, and will improve the heat transfer. Radial strips, however, will face the airflow at an oblique angle. This will lengthen the effective strip width, and may slightly reduce the heat transfer. Youn et al. [2003] investigated the performance of the radial strip geometry having 1.5-mm strip width. The data were compared with those of Du and Wang [2000], which had 1.0-mm width strips formed normal to the flow direction. The slit area fractions of both geometries were approximately the same (0.47 for the radial strips and 0.45 for the normal strips). The results showed that the j and f factors were approximately equal. It is likely that the pros and cons of the two geometries cancel each other, yielding approximately the same j and f factors.

Several correlations are available to predict the j and f factors of OSF heat exchangers (Nakayama and Xu [1983], Kang and Webb [1998], Wang et al. [1999b], Du and Wang [2000], Youn et al. [2003]). The geometry range of the correlations are, however, very limited, because most of them were developed using a small database of the investigators data. An interesting correlation concept has been proposed by Kang and Webb [1998]. They correlated their data using the strip area fraction. They show that the j factor increases as the strip area increases. The concept has also been used by Youn et al. [2003]. Currently, no general correlation is available.

6.5.3 Convex Louver Fins

Hitachi [1984] uses the convex louver fin geometry in its commercial plate fin-and-tube heat exchangers. Figure 6.2d is taken from the Hitachi [1984] product brochure. The performance of the convex louver fin plate-and-fin surface geometry was compared to the OSF geometry in Section 5.4. Hatada et al. [1989] report performance data of the Figure 6.2d type fin geometry for a one-row heat exchanger. Figure 6.8 illustrates the finned tube geometry, and Figure 6.9 shows the air-side h and Δp values vs. air velocity for three geometries tested. The geometry details of the three Figure 6.9 geometries are defined on Figure 6.8. Figure 6.9 shows data for two variants of the convex louver fin geometry. Fin number 2 has a uniform convex louver shape (louver angle $\theta_1 = 12.5°$). Fin number 1 has $\theta_1 = 17.5°$ in the regions between the tubes (between sections B-B and C-C on Figure 6.8), and $\theta_2 = 40°$ adjacent to the tubes. The reduced louver angle near the tubes allows more airflow in the vicinity of the tubes. The 17.5° louver angle in the fin region between the tubes was found to give high j and j/f by Hatada and Senshu's [1984] studies of the plate-and-fin geometry, as discussed in Section 5.4. Figure 6.9 shows that the number 1 fin geometry gives approximately 10% higher h value than the number 2 fin geometry. The h value of the number 1 louver fin geometry is 2.85 times that

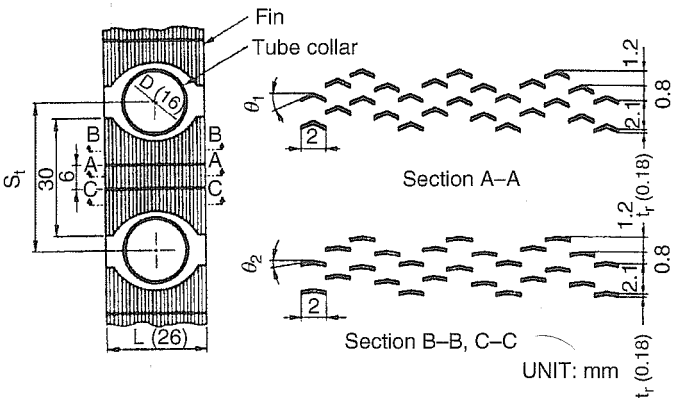

Figure 6.8 Convex louver plate fin-and-tube geometry tested by Hatada et al. [1989].

of the plain fin (number 3) at the same air velocity. When compared at the same air friction power, the h value of the number 1 fin is 2.3 times that of the number 3 plain fin.

The effect of fin pitch and tube rows on the j and f factors of the convex louver geometry have been investigated by Wang et al. [1996a, 1998a]. The samples had 15.5° convex angle. The trends were similar to those of the wavy fin geometry, which showed that the j factors were independent of fin pitch. The row effect on the j factors was relatively weak compared with that of the plain fin geometry. The friction factors were independent of the number of tube rows. The j and f factors of the convex louver fin heat exchangers showed a 21 to 41% and 60 to 72% increase as compared to the corresponding wavy fin geometry. The performance of the convex louver fin geometry was compared with the louver and wavy fin geometries. Based on the volume goodness comparison method (see Section 3.10.1), the convex louver geometry yielded the best performance, followed by the louver and the wavy fin geometries.

6.5.4 Louvered Fin

The louver geometry discussed in Section 5.3 has been applied to finned-tube heat exchangers. Louver patterns are formed on the fin area between tubes. Care must be exercised in louvering the fin surface, because the louvers can cut the conduction path from the tube. The air-side performance of louvered fin heat exchangers has been investigated by Wang and co-workers (Chang et al. [1995], Wang et al. [1998b, 1999e]). Their study included six different louver geometries, 1.21 mm $\leq p_f \leq$ 2.49 mm, one to six rows. Similar to the other geometries such as plain or wavy fin, the j factors were independent of fin pitch. The effect of the number of tube rows was negligible for Re_d >2000. However, significant reduction of the j factor with increasing number of tube row was found for the lower Reynolds numbers. The row effect is discussed in detail in Rich [1975] for plain fins, and also shown in Figure 6.5.

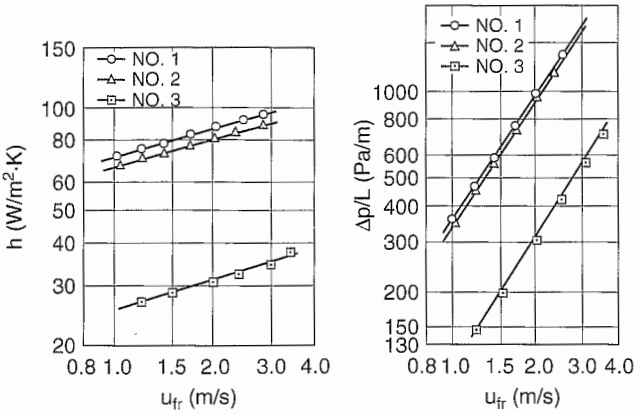

Heat Exchanger Dimensions

	Convex strip fin		Plain plate fin
Feature	Fin no. 1	Fin no. 2	Fin no. 3
Transverse tube pitch S_t (mm)	38	38	36
Fin depth L (mm)	26	26	42
Number of rows	1	1	1
Tube diameter d (mm)	16	16	16
Fin pitch p_f (mm)	2.2	2.2	2.1
Fin thickness t (mm)	0.18	0.18	0.18
Ramp angle θ_1 (Degrees)	17.5	12.5	—
Ramp angle θ_2 (Degrees)	40	12.5	—

Figure 6.9 Performance data for the Figure 6.7 convex louver surface geometries of Hatada et al. [1989].

The friction factors were independent of the tube rows. Wang et al. [1999e] developed j and f correlations based on their data.

The two most widely used enhanced geometries in the air-conditioning and refrigeration heat exchangers are the slit and louvered fins. Wang et al. [2001] compared the performances of the state-of-the-art configuration of the two geometries. Various comparison methods were tried; the volume goodness comparison, VG-1 cirterion in Table 3.1, etc. The two geometries yielded comparable results. Hence, one cannot conclude that one basic geometry is better than the other. Their performance will be dependent on the louver (or slit) pitch, and the fraction of the fin area on which louvers (or slits) exist.

6.5.5 Perforated Fins

Fujii et al. [1991] tested a plate-fin geometry made of corrugated, perforated plates whose fin geometry is illustrated in Figure 5.25. Section 5.7 discusses the performance of this geometry as a plate-and-fin heat exchanger configuration. Fujii et al. [1991] applied the Figure 5.25 surface to a one-row plate-fin heat exchanger having 0.5-mm-thick copper fins, and obtained experimental results. Their heat exchanger was made of 28-mm-diameter tubes at 76-mm tube pitch and 66-mm fin depth. Figure 6.10 defines the geometry details, and presents the test results for the 2 fin geometry variants, each for 6.0- and 8.0-mm fin pitch. Fin geometries number 1 and number 3 are the same, as are number 2 and number 4. Both fin geometry variants provide approximately equal Nu. However, geometry number 3 provides a lower friction factor than geometry number 4 (6-mm fin pitch). Although the Nu is

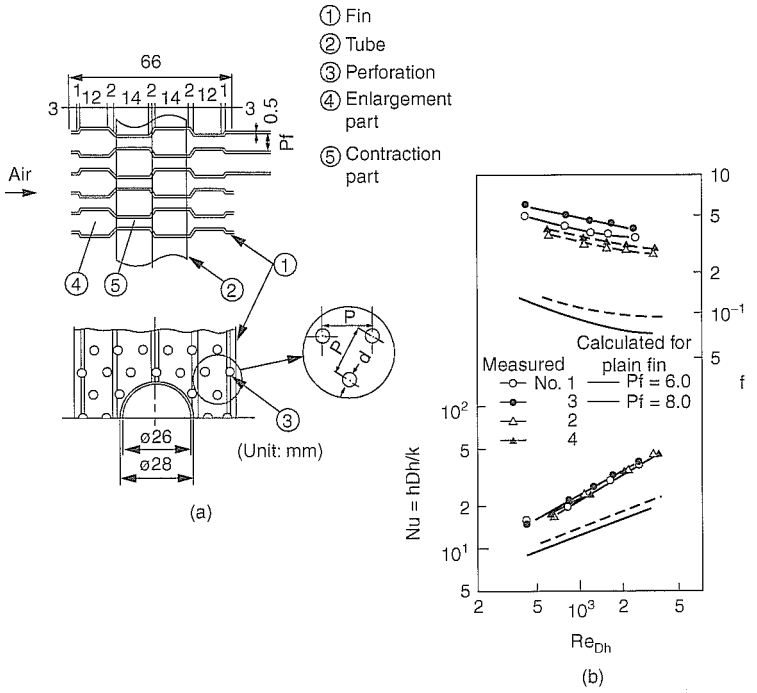

Geom.	P_f (mm)	P (mm)	d (mm)	σ	β
1	6	5	2	0.29	0.145
2	8	5	2	0.43	0.145
3	6	10	3	0.29	0.082
4	8	10	3	0.43	0.082

Figure 6.10 (a) Illustration of one-row finned-tube heat exchanger tested by Fujii et al. [1991], (b) air-side test results.

increased approximately 100%, the friction factor of geometry number 3 is increased a factor of 2.3, relative to a plain fin. This friction performance is not competitive with other high-performance fin geometries discussed in this chapter. Note that the Figure 6.10 data may be scaled to other tube diameters by scaling all the dimensions in the ratio of the new and original tube diameters.

6.5.6 Mesh Fins

The mesh fin geometry described in Chapter 5.8 has been applied to circular finned-tube heat exchangers. A good design copper mesh fin heat exchanger using 4-mm-diameter tubes yields approximately 100% higher heat transfer at the same pumping power than conventional louver fin heat exchangers (Ebisu [1999]). The high heat transfer coefficient of the mesh fin, small tube diameter (4 to 5 mm), and large surface-to-volume ratio of the mesh fin heat exchanger lead to the high performance. Extending the work of Torikoshi and Kawabata [1989] for a mesh fin heat exchanger with inline fin coniguration, Ebisu [1999] investigated the effect of offsetting the fin array ($0.0 \le a/m \le 0.5$) for 6 layers of mesh having dimensions $d = 0.2$ mm, $m = 2.3$ mm, $l = 5.0$ mm, where m is the distance between slits and a is the offset length of the succeeding fin (shown in Figure 5.27). The mesh fins were soldered to 4.0-mm-diameter tubes having 20-mm pitch. The heat transfer coefficient increased as the degree of offset increased. The $a/m = 0.0$ corresponds to inline fin configuration. The heat transfer enhancement obtained by 50% offsetting the fin array ($a/m = 0.5$) was 134%, when compared with results for the inline arrangement ($a/m = 0$). The corresponding increase of the pressure drop was 40%. Ebisu [1999] also investigated the effect of tube arrangement ($0.0 \le y/P_t \le 0.5$), where y is the offset distance of the downstream tube from inline position. The $y/P_t = 0.0$ and 0.5 corresponds to inline and staggered tube layouts, respectively. The largest heat transfer coefficient was obtained for $0.25 \le y/P_t \le 0.35$. The pressure drop was also the highest in that range. Figure 6.11 shows the flow visualization results for three-row tube bundles having different offsets. Figure 6.11 shows that, for $y/P_t = 0.0$ and 0.1, the tubes at the second and subsequent rows are surrounded by the separated flow from upstream tubes. For $y/P_t = 0.5$, the tubes in the third row are under the influence of the wakes from the first row. For $y/P_t = 0.25$, the downstream tubes are not influenced by the wakes.

In Figure 6.12, the performance of copper mesh finned heat exchangers are compared with copper or aluminum louver fin heat exchangers ($d_o = 9.5$ mm, $P_t = 25.4$ mm). Note that the mesh fins are attached to a 4.0-mm tube. In Figure 6.12, hA/V is the heat transfer per unit volume, and P/V is the pumping power per unit volume. Figure 6.12 shows that the hA/V values of good-design mesh finned heat exchangers having offset fin array and staggered tube layout (shown as large symbols in the figure) are approximately twice as high as that for the aluminum louver fin heat exchanger at the same pumping power.